Evaluation of Polycyclic Aromatic Hydrocarbon Formation in Counterflow Diffusion Flames

R. Tripathi[1,*], *W. Pejpichestakul*[2], *L. Cai*[1], *M. Pelucchi*[2], *T. Faravelli*[2], *H. Pitsch*[1]

[1]Institute for Combustion Technology, RWTH Aachen University, 52056 Aachen, Germany
[2]CRECK Modeling Laboratory, Department of Chemistry, Materials and Chemical Engineering "G. Natta", Politecnico di Milano, Italy

Abstract

Polycyclic aromatic hydrocarbons (PAHs) have been heralded as mutagenic and carcinogenic substances and currently, their emissions are subject to regulatory control due to recently imposed stricter environmental regulations. Hence, it has become necessary to have a detailed understanding of their chemistry. In this work, a short review of the available PAH relevant counterflow diffusion flame datasets is presented. Following that, the reliability of four widely used PAH mechanisms and the revised PAH mechanism, within the scope of this work, is assessed by validating them against these collected experimental datasets. The formation of the first aromatic ring is investigated based on the performed reaction path analyses. The results show that the dominant reaction pathways for the formation of benzene are "even carbon atom" pathways (H-abstraction acetylene addition) and "odd carbon atom" pathways (recombination of propargyl radicals). The dominance of one pathway over the other was found to be strongly dependent on the fuel structure and its doping with other components.

1. Introduction

There is an increased concern about the occurrence of polycyclic aromatic hydrocarbons (PAHs) in the environment as they are amongst the strongest known carcinogens [1]. These pollutants are associated with particulate carbonaceous materials resulting from the incomplete combustion of transportation fuels [2]. A considerable amount of effort has been put into the formation and growth of soot particles in flames and their modeling [3–6]. However, various studies reveal that for predicting soot formation it is essential to predict their precursors accurately [4], i.e., the formation and growth of PAH at molecular level. Regarding PAH formation and growth, Pejpichestakul et al. [7] summarized various experimental studies on burner stabilized premixed flames in their recent publication. Apart from that, a revised chemical kinetic model of PAH was presented and the importance of soot chemistry in the PAH mechanism was discussed. Although several studies focusing on the formation and growth of PAHs in burner stabilized premixed flame exist, numerical simulations for these flames cope up with uncertainties since the boundary conditions for these flames are difficult to determine. As a result, temperature profiles are usually specified rather than being computed. On the contrary, counterflow diffusion flames are excellent candidates to mimic the non-premixed combustion mode in diesel engines, fire, and furnaces. Moreover, the flames stay away from any walls or surfaces, hence uncertainties resulting from boundary conditions are minimized. Prompted by this insight, this work first presents a short review of the available PAH relevant counterflow diffusion flames. Then, the available data for various hydrocarbon fuels are used to critically assess the performance of the existing PAH models and the revised model in the present work. The main formation pathways for PAH precursors and main PAH species have been analyzed. Particular attention has been given to the formation of the first aromatic ring.

2. Experimental database

As part of a broad investigation on the PAH formation and growth in non-premixed combustion mode, the present study includes 30 counterflow diffusion flames from 7 different references [8–14]. Baroncelli et al. [8] investigated the formation of PAH species in pure acetylene flame and methane doped acetylene flame at atmospheric pressure. In addition to C_1 to C_5 species, several mono-aromatic (e.g., benzene, toluene, and styrene) and bi-aromatic (e.g., indene and naphthalene) species were quantified. Carbone et al. [9] studied the effect of pressure variation on incipiently sooting counterflow flames of ethylene, 9 flames in a pressure range of 1 atm to 8 atm were measured. Along with the smaller species, main quantified PAH species include benzene, toluene, indene, phenylacetylene, and naphthalene. Considered flames from the third reference include the measurements of PAH species in ethylene flames at high pressures from the study of Figura et al. [10]. Various mono-aromatic species like benzene, toluene, styrene, and xylene were detected in their measurements. Carbone et al. [10] also investigated the PAH formation in toluene doped methane flame, toluene doped ethylene flame, and in correspond-

* Corresponding author: r.tripathi@itv.rwth-aachen.de

Table 1: Counterflow diffusion flame datasets.

No.	Fuel	P [atm]	PAH species	Ref.
1	C_2H_2	1	up to A2	[8]
2	C_2H_2/CH_4	1	up to A2	[8]
3-11	C_2H_4	1-8	up to A2	[9]
12-17	C_2H_4	1-8	up to A1	[10]
18	CH_4/Toluene	0.4	up to A1	[11]
19	C_2H_4/Toluene	0.4	up to A1	[11]
20-22	C_2H_2	1	only benzene	[12]
27	1,3-Butadiene	1	up to A1	[13]
28-30	*n*-Heptane	1	only benzene	[14]

ing baseline flames in a separate study. Molar concentrations of several mono-aromatic species, benzene, toluene, xylene, styrene, phenylacetylene, ethylbenzene, and propylbenzene, were reported. out of the remaining three studies, the work of the Moshammer et al. [13] includes measurement of PAH species in a butadiene flame at nearly atmospheric pressure. PAH species up to naphthalene were identified and reported. Other two studies, one by Leusden et al. [12] and the other by Berta et al. [14], do not include species forming as a result of PAH growth and only the concentration of benzene was reported. The study of Leusden et al. [12] includes the measurements of benzene in an acetylene flame and the experimental database on counterflow diffusion flame of acetylene is scarce that is why this flame was included in our database. The reason for including the experimental data of Berta et al. [14] is to assess the formation of the first aromatic ring in an *n*-heptane flame, which is a conventional fuel component. A list of considered flames has been summarized in Table 1.

3. Mechanisms

A number of detailed mechanisms consisting PAH chemistry have been developed during the last years. In the present work, the most widely used PAH mechanisms, which have been tested against comprehensive datasets obtained in flames and canonical combustion reactors, have been considered. A brief overview of the mechanisms considered in the present work is as follows:

- In 2000, a soot formation mechanism consisting of detailed PAH chemistry was presented by Appel et al. [15]. This mechanism was based on the previous mechanism of Wang and Frenklach [16] and several modifications based on the available literature on gas phase reactions were incorporated. Of all 101 species in the model, 34 were aromatic species. The PAH aromatic-ring growth was based on the H-abstraction-C_2H_2-addition (HACA) reaction sequence, therefore many aromatic species having odd carbon numbers were not present in the model. This model was tested against species profiles of major and minor chemical species, aromatics, soot volume fractions, and soot particle diameters reported in the literature for nine laminar premixed flames of ethane, ethylene, and acetylene. This mechanism will be addressed as the ABF mechanism in the this stuty.

- Later, in 2013 Wang et al. [17] developed a detailed PAH reaction mechanism, which includes the formation and growth of PAHs up to coronene ($C_{24}H_{12}$). This mechanism is quite extensive and contains 81 aromatic species including odd carbon number aromatic species. In the same work itself, the performance of the mechanism was evaluated by validating it against the PAH species profiles obtained in various burner-stabilized premixed flames and counterflow diffusion flames of fuels with smaller carbon chain, up to C_3. This mechansim will be addressed as the KAUST mechansim in this work.

- In 2015, Narayanaswamy et al. [18] presented a detailed PAH mechanism, which was based on their previously published PAH mechanism [19] and included the revised H_2/O_2 chemistry. This mechanism describes the moderate to high-temperature oxidation of several aromatics, viz. toluene, ethylbenzene, styrene, xylene, methylnaphthalene, and pyrene and contains 41 aromatic species. Various isomers of aromatic species were considered and odd number aromatic species were also available in the model. Extensive validation of the mechanism was done by comparing it against plug flow reactor data, ignition delay times, species profile measurements, and laminar burning velocities [18, 19]. This mechanism will be addressed as the ITV mechanism in the present work.

- Recently, Pejpichestakul et al. [7] extended the core C_0–C_2 mechanism up to the kinetic mech-

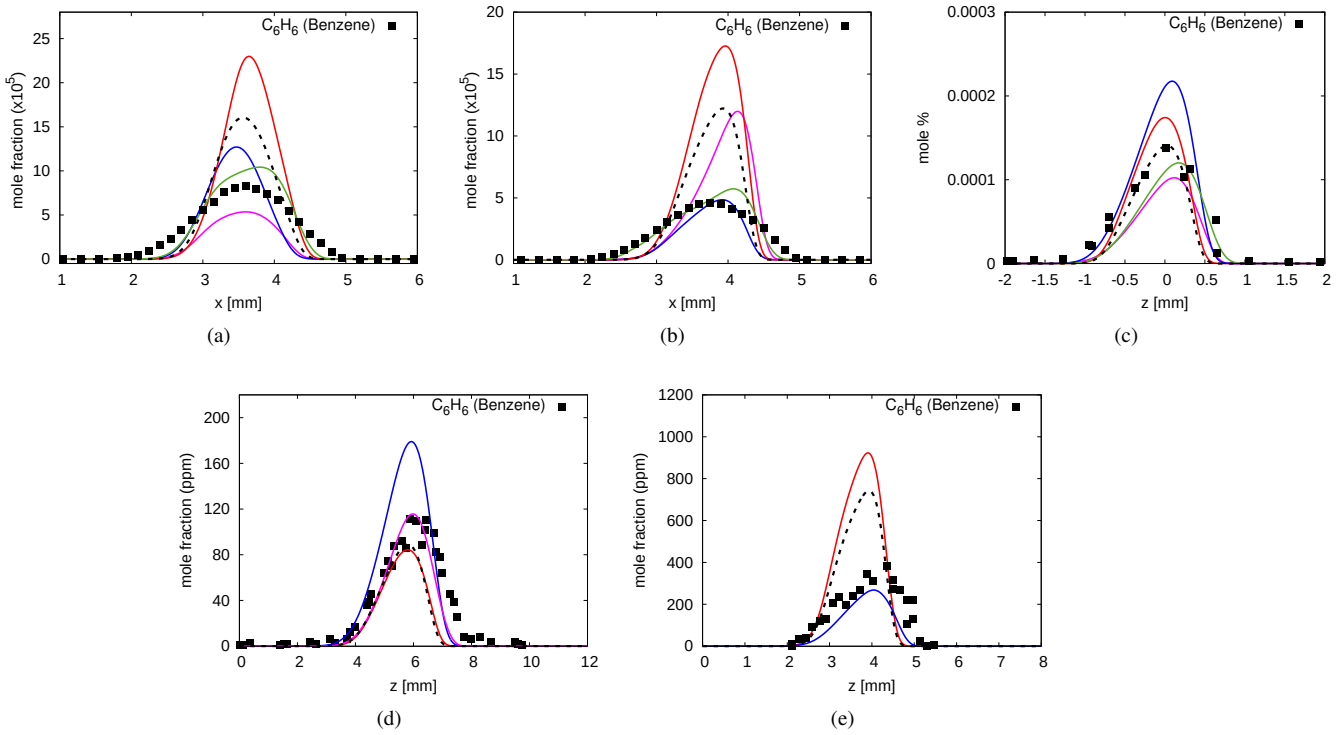

Figure 1: Comparison between experimental (symbols) and predicted (lines) benzene profiles. Figure (a) acetylene flame at P = 1 atm [8]; (b) methane doped acetylene flame at P = 1 atm [8]; (c) ethylene flame at P = 1 atm [9]; (d) toluene doped ethylene flame at P = 0.4 atm [10]; (e) *n*-heptane flame at P = 1 atm [14]. Green solid lines (——) represent the ABF model, magenta solid lines (——) represent the KAUST model, red solid lines (——) represent the ITV model, blue solid lines (——) represent the CRECK model, and black dashed lines (- - -) represent the updated ITV model.

anism of PAH and soot formation based on the previously published mechanisms within their research groups. This mechanism consists of 38 aromatic species and includes odd carbon number species too. This is the most recent and extensively validated mechanism in the literature since it was validated against the PAH species profiles from 60 different burner stabilized premixed flames. However, the CRECK mechanism adopted in this work neglects the soot sub-mechanism. This mechanism will be addressed as the CRECK mechanism in the current work.

- In the present work, the ITV mechanism was revised based on the recent theoretical studies on the PAH relevant reactions and the improvisements, which were already involved in the CRECK mechanism and were missing in the ITV mechanism were incorporated. In particular, two major revisions were included, the incorporation of recently calculated rate parameters for H-abstraction by H from various mono- and bi-cyclic aromatic species [20] and the incorporation of pressure dependent rate parameters for several reactions. This mechanism will be addressed as the updated ITV mechanism in the following sections.

4. Results and discussion

Numerical simulations including mixture-averaged transport parameters and thermodiffusion were performed using the FlameMaster [21] code. All validation cases listed in Table 1 were considered for the evaluation of the performance of the mechanisms. However, for the sake of brevity, only the mono-aromatic ring formation in five different flames is presented in the present work. Five chosen flames include the pure acetylene flame of Baroncelli et al. [8], methane doped acetylene flame of Baroncelli et al. [8], the ethylene flame of Carbone et al. [9], toluene doped ethylene flame of Carbone et al. [10], and *n*-heptane flame of Berta et al. [14]. Figure 1 shows the comparison of numerically calculated species profiles of benzene against the measured ones.

As can be seen in Fig. 1a, all the tested mechanisms predict the concentration of benzene in acetylene flame reasonably well except the ITV mechanism. A similar prediction was observed in methane doped acetylene flame too (Fig. 1b), however here the KAUST mechanism also over-predicts the benzene concentration. The prediction of the benzene formation in acetylene flames were found to be linked with the prediction of the vinylacetylene concentration. It can be seen in Fig. 2a that the concentration of vinylacetylene is predicted reasonably well by the ITV mechanism and over-predicted by the CRECK mechanism, whereas the trend for the prediction of the benzene formation is opposite from these

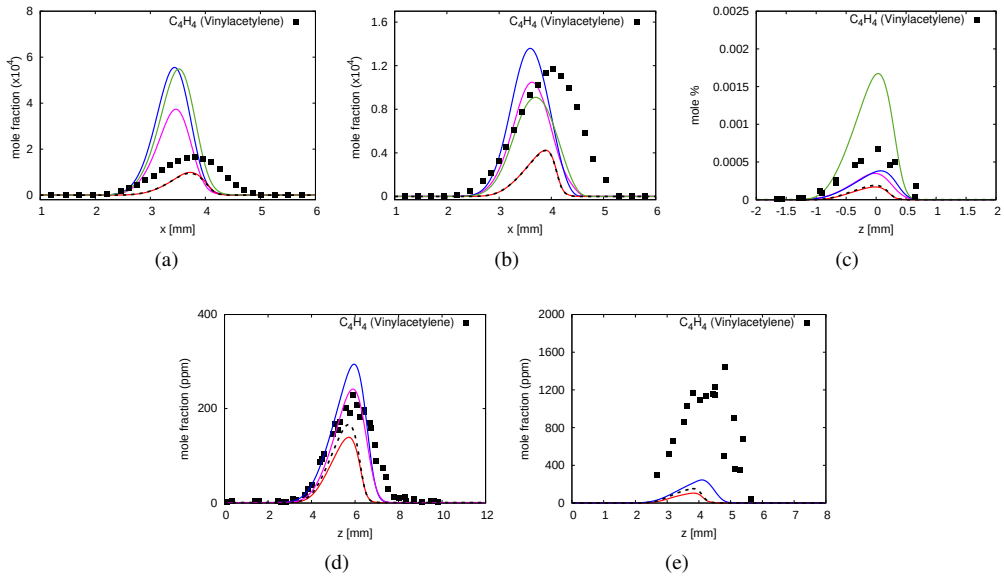

Figure 2: Comparison between experimental (symbols) and predicted (lines) vinylacetylene (C_4H_4) profiles. Figure (a) acetylene flame at P = 1 atm [8]; (b) methane doped acetylene flame at P = 1 atm [8]; (c) ethylene flame at P = 1 atm [9]; (d) toluene doped ethylene flame at P = 0.4 atm [10]; (e) *n*-heptane flame at P = 1 atm [14]. Green solid lines (——) represent the ABF model, magenta solid lines (——) represent the KAUST model, red solid lines (——) represent the ITV model, blue solid lines (——) represent the CRECK model, and black dashed lines (- - -) represent the updated ITV model.

two mechanisms. Figs. 1c and. 1d represent the benzene concentration in an ethylene flame [9] and in a toluene doped ethylene flame [10], respectively. In both flames, the ITV mechanism predicts the max concentration of benzene well and the CRECK mechanism shows a slight over-prediction. Looking at the vinylacetylene profiles in these two flames (Figs. 1c and 1d) it can be concluded that the link between benzene and vinylacetylene concentration depends on the fuel. In ethylene flame, vinylacetylene is reasonably predicted by all the mechanisms except the ABF mechanism, which over-predicts it. The comparison of the ABF mechanism against the vinylacetylene profile is not shown in Fig. 2d since this is a toluene doped ethylene flame and toluene is not present in that mechanism. The last benzene profile presented in Fig. 1e was measured in an *n*-heptane flame. The KAUST mechanism and the ABF mechanism does not include *n*-heptane, hence comparisons are made only with the ITV and the CRECK mechanisms. Similar to the acetylene flame, the ITV mechanism over-predicts the benzene concentration in the *n*-heptane flame and the CRECK mechanism shows good agreement. The concentration of vinylacetylene in *n*-heptane flame is under-predicted by the ITV mechanism as well as by the CRECK mechanism. The performance of the revised mechanism (black dashed lines) is improved for all the flames in comparison to the ITV mechanism ((Fig. 1) without altering the prediction of vinylacetylene concentration (Fig. 2). However, prediction accuracy in acetylene and *n*-heptane flames is not as good as that by the CRECK mechanism. This mechanism is still under revision and future work will include several other updates based on the recent literature on gas-phase PAH kinetics.

In order to analyze the pathways forming the first aromatic ring, reaction path analyses were performed for all five flames using the updated ITV mechanism and are shown in Fig. 3a. As can be seen in Fig. 3a, neglecting the inter-conversion of phenyl to benzene and vice versa, acetylene addition to the butadienyl radical (HACA) is the main formation pathway of benzene in the acetylene flame. A major concentration of butadienyl radical comes from vinylacetylene and hence formation pathways of vinylacetylene and their precursors play an important role in the prediction of benzene and need to have accurate rate parameters in the mechanism. In contrast to acetylene flame, the main benzene formation pathway in methane doped acetylene flame is the recombination of propargyl radicals, Fig. 3b. The reason behind this is the increased concentration of singlet methylene (S-CH_2) radical since $CH_3 + H = S\text{-}CH_2 + H_2$ is a major formation route of S-CH_2 and the main formation route of propargyl radical is C_2H_2 + S-CH_2 = C_3H_3 + H. In both ethylene and toluene doped ethylene flame the recombination of propargyl is the main rate-limiting step for the formation of the first aromatic ring (see Figs. 3c and 3d). However, the contribution of these pathways for the first ring formation substantially increases in the *n*-heptane flame (Fig. 3e).

5. Concluding remarks

With the objective of a better and updated kinetic model for PAHs, four widely used PAH reaction mechanisms have been used to simulate the formation of the first aromatic ring in a set of counterflow laminar diffusion flames. Depending on the fuel's structure, the prediction of the concentration of benzene has been found to be re-

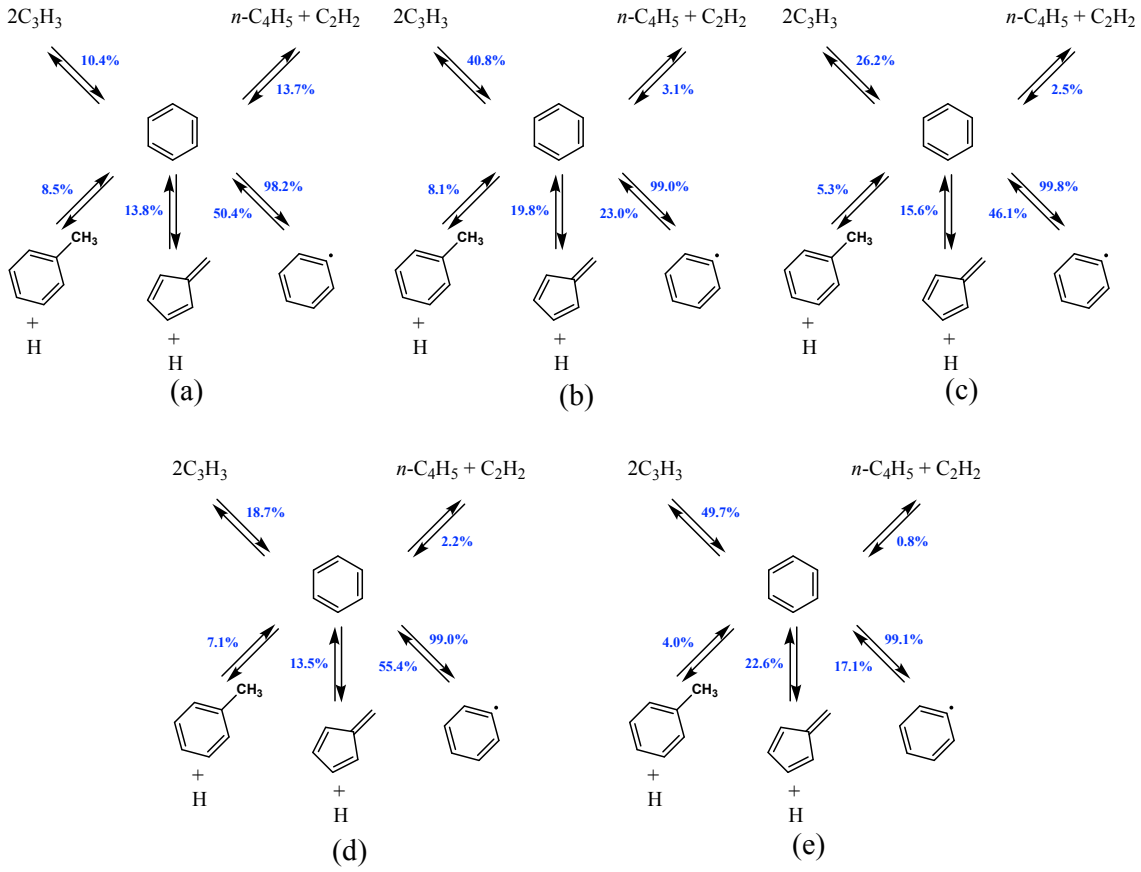

Figure 3: Main reaction pathways forming benzene in five different counterflow diffusion flames. Figure (a) acetylene flame at P = 1 atm [8]; (b) methane doped acetylene flame at P = 1 atm [8]; (c) ethylene flame at P = 1 atm [9]; (d) toluene doped ethylene flame at P = 0.4 atm [10]; (e) *n*-heptane flame at P = 1 atm [14].

lated to the prediction of the vinylacetylene. Especially in acetylene, methane doped acetylene, and *n*-heptane flames. For these flames, benzene formation is over-predicted by the ITV mechanism and predicted well by the CRECK mechanism. Whereas, the prediction of the formation of the first ring in ethylene and toluene doped ethylene flames is predicted well by the ITV mechanism and over-predicted by the CRECK mechanism. The performed flux analysis reveals the importance of the C_3 and C_4 species for the formation of the first ring. Therefore, reactions involving the formation of these species and their precursors should be considered as important targets of revision in future work. In addition to the literature mechanisms, in the present work, the ITV mechanism was revised and was also employed for the validation of the collected flame datasets. The performance of the revised model is improved in comparison to the previous ITV model. This mechanism is still under revision and future work will incorporate missing pathways, which are already available in other mechanisms. Also, the revision of the rate parameters of sensitive pathways for the formation of the first PAH ring and its growth to higher carbon species will be done based on the literature recommendations.

Acknowledgments

This work was supported by The Computational Chemistry Consortium (C3).

References

[1] C.-E. Boström, P. Gerde, A. Hanberg, B. Jernström, C. Johansson, T. Kyrklund, A. Rannug, M. Törnqvist, K. Victorin, R. Westerholm, Environ. Health Perspect. 110 (2002) 451–488.

[2] L. Morawska, J.J. Zhang, Chemosphere 49 (2002) 1045–1058.

[3] H. Wang, Proc. Combust. Inst. 33 (2011) 41–67.

[4] R.A. Dobbins, R.A. Fletcher, H.-C. Chang, Combust. Flame 115 (1998) 285–298.

[5] A. Veshkini, N.A. Eaves, S.B. Dworkin, M.J. Thomson, Combust. Flame 167 (2016) 335–352.

[6] M.E. Mueller, G. Blanquart, H. Pitsch, Combust. Flame 156 (2009) 1143–1155.

[7] W. Pejpichestakul, E. Ranzi, M. Pelucchi, A. Frassoldati, A. Cuoci, A. Parente, T. Faravelli, Proc. Combust. Inst. 37 (2019) 1013–1021.

[8] M. Baroncelli, D. Felsmann, N. Hansen, H. Pitsch, Investigating the effect of oxy-fuel combustion and light coal volatiles interaction: a mass spectrometric study, Combust. Flame submitted.

[9] F. Carbone, K. Gleason, A. Gomez, Proc. Combust.

Inst. 36 (2017) 1395–1402.
[10] L. Figura, A. Gomez, Combust. Flame 161 (2014) 1587–1603.
[11] F. Carbone, A. Gomez, Combust. Flame 159 (2012) 3040–3055.
[12] C.P. Leusden, N. Peters, Proc. Combust. Inst. 28 (2000) 2619–2625.
[13] K. Moshammer, L. Seidel, Y. Wang, H. Selim, S.M. Sarathy, F. Mauss, N. Hansen, Proc. Combust. Inst. 36 (2017) 947–955.
[14] P. Berta, S.K. Aggarwal, I.K. Puri, Combust. Flame 145 (2006) 740–764.
[15] J. Appel, H. Bockhorn, M. Frenklach, Combust. Flame 121 (2000) 122–136.
[16] H. Wang, M. Frenklach, Combust. Flame 110 (1997) 173–221.
[17] Y. Wang, A. Raj, S.H. Chung, Combust. Flame 160 (2013) 1667–1676.
[18] K. Narayanaswamy, H. Pitsch, P. Pepiot, Combust. Flame 162 (2015) 1193–1213.
[19] K. Narayanaswamy, G. Blanquart, H. Pitsch, Combust. Flame 157 (2010) 1879–1898.
[20] D. Hou, X. You, Phys. Chem. Chem. Phys. 19 (2017) 30772–30780.
[21] H. Pitsch, Flamemaster: A C++ Computer Program for 0D Combustion and 1D Laminar Flame Calculations, (1993).